

LASER ENERGY CONVERSION TO SOLITONS AND MONOENERGETIC PROTONS IN NEAR-CRITICAL HYDROGEN PLASMA*

I. V. Pogorelsky[#], M. Babzien, M. N. Polyanskiy, V. Yakimenko, BNL, Upton, New York, USA,
 N. P. Dover, C. A. J. Palmer, Z. Najmudin, J. Schreiber, Imperial College, London, UK
 M. Ispiryan, P. Shkolnikov, SUSB, Stony Brook, New York, USA,
 G. Dudnikova, UMD, College Park, Maryland, USA.

Abstract

Recent theoretical and experimental studies point to better efficiency of laser-driven ion acceleration when approaching the critical plasma density regime. Simultaneously, this is the condition for observing solitons: "bubble"-like quasi-stationary plasma formations with laser radiation trapped inside. Exploring this regime with ultra-intense solid state lasers is problematic due to the lack of plasma sources and imaging methods at $\sim 10^{21}$ cm⁻³ electron density. The terawatt picosecond CO₂ laser operated at Brookhaven's Accelerator Test Facility offers a solution to this problem. At the 10 μ m laser wavelength, the critical plasma density is 10^{19} cm⁻³, which is attainable with gas jets and can be optically probed with visible light. Capitalizing on this approach, we focused a circular-polarized CO₂ laser beam with $\alpha_0=0.5$ onto a hydrogen gas jet and observed monoenergetic proton beams in the 1 MeV range. Simultaneously, the laser/plasma interaction region has been optically probed with a 2nd harmonic picosecond Nd:YAG laser to reveal hole boring and stationary soliton-like plasma formations. 2D PIC simulations agree with experimental results and aid in their interpretation.

INTRODUCTION

On its route to practical applications, research on laser acceleration of ions has to find ways for better converting the laser beam energy to directed proton beams of a narrow energy spread. In a vast majority of laser-ion acceleration experiments, the dominant mechanism of ion acceleration has been Target Normal Sheath Acceleration (TNSA) [1]. While TNSA process starts from electron heating by the laser pulse, it ultimately results in well-collimated, high-energy ion beams of significant brightness. However, the ion energy spectra are in general too broad for many important applications.

A different regime of ion acceleration called Radiation Pressure Acceleration (RPA) [2,3] provides an alternative route to producing laser-driven monoenergetic ion beams with faster energy scaling ($\sim I$, as opposed to $\sim I^{1/2}$ for TNSA) [2,3,4] that promises to facilitate attaining relativistic ion energies. This mechanism is possible when the conditions are met for direct laser energy deposition to the critical plasma surface pushed by the radiation pressure. Only at very high field intensities ($>10^{22}$ W/cm²

for $\lambda \sim 1 \mu$ m lasers), unavailable yet, the RPA mechanism becomes more pronounced than TNSA. Fortunately, RPA may be investigated at much lower intensities if one utilizes laser beams with circular polarization, which strongly suppresses electron heating, and longer wavelength that allows to utilize less dense plasmas.

In this paper, we report the first to our knowledge experimental observation of RPA using a circularly polarized CO₂ laser with $\lambda=10 \mu$ m focused upon a supersonic hydrogen gas jet. Gas jets offer viable alternative to solid foil targets because they facilitate high repetition-rate operation and allow easy adjusting the target density and material. However, gas jets have limited operating density range, being particularly difficult to operate near or above critical plasma density, which is necessary for RPA [5] (for a 1- μ m laser, $n_c = \pi / (r_e \lambda^2) = 10^{21}$ cm⁻³, where $r_e \approx 2.8 \times 10^{-13}$ cm is the classical electron radius). This can be remedied by using longer wavelength infrared lasers. For example, for a 10- μ m CO₂ laser, $n_c = 10^{19}$ cm⁻³. This density is easily obtained in a gas jet. In addition, the low-density plasma lends itself to much wider array of diagnostic tools, including optical lasers. This opens a unique possibility for investigating a broad variety of phenomena occurred at laser interaction with near- and over-critical plasma such as filamentation instability, self-focusing, soliton formation, hole boring, and so on.

Capitalizing on aforementioned benefits of a gas jet and a CO₂ laser combination, we scanned over a range of plasma densities above and below n_c . Our prime goal was finding the optimum conditions for producing monoenergetic proton beams via RPA. Simultaneously, by implementing an optical diagnostic technique, we visualized plasma response to the laser energy deposition at different interaction conditions. This approach allowed us to demonstrate the record proton monochromaticity ($\sigma \approx 4\%$) obtained in the RPA hole-boring regime as well as the first optical imaging of post-solitons as is further addressed in this paper.

EXPERIMENT AND SIMULATIONS

Experimental Layout

Fig. 1 describes the setup of an experiment designed to study radiation driven ion acceleration from gas targets with a CO₂ laser. The experiment was performed at the Accelerator Test Facility in Brookhaven National Laboratory by a collaboration led by Imperial College. A 5 ps, 1 TW CO₂ laser pulse was focused by an f/3 off-axis

*Work supported by Libra Basic Technology Consortium and US DOE grant DE-FG02-07ER41488...

[#]igor@bnl.gov

parabolic mirror onto the front surface of a supersonic hydrogen gas jet with a 1mm opening aperture. Intensities of $\sim 10^{16}$ W/cm² were reached in a focal spot of the $w_0=60$ μ m radius. The proton beam, accelerated along the laser axis, was diagnosed using a simple magnetic spectrometer with the 0.6 mm diameter entrance pinhole and polyvinyltoluene scintillator coupled to an EMCCD.

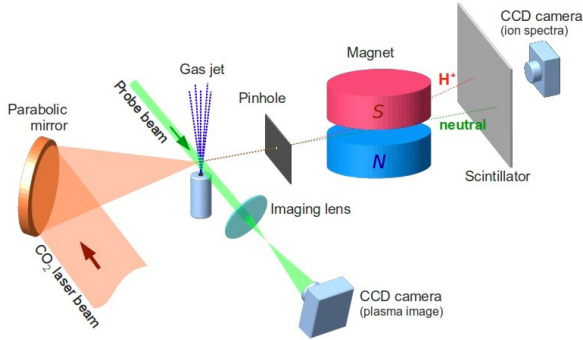


Figure 1: Layout of experiment.

A frequency doubled Nd:YAG probe beam ($\lambda=532$ nm) of the 14 ps pulse length provided magnified interferometry and shadowgraphy images of the interaction region. Information about the ionization of the gas jet and density maps of the plasma were obtained by analysis of the fringe shifts on the interferometry images. A similar method was also used to determine the correlation between the backing pressure and the density distribution in the gas jet. An example of gas density distribution for 600 psi hydrogen backing pressure is shown in Fig.2. The radial profile of the gas density along the laser beam propagation has a triangular shape with the maximum density on the jet axis that scales linearly with the backing pressure.

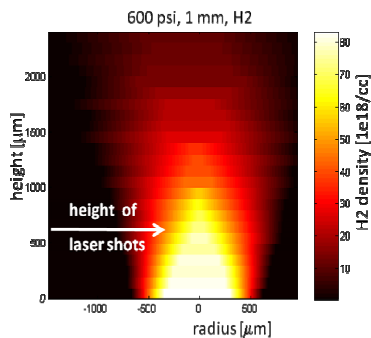


Figure 2: Gas density profile in a jet.

Simulations

To model the interaction, 2D PIC simulations of the dynamics of laser-plasma interaction have been performed. The simulation box is $45\lambda \times 40\lambda$, with mesh resolution of 16 cells per laser wavelength, λ . The number of quasiparticles is 4×10^4 . The target is made of hydrogen plasma, and localized between $5\lambda < x < 37\lambda$. The plasma density of the target has triangular shape, unless specified otherwise. A circularly polarized laser pulse has a

Gaussian shape with a length of $\tau=50\lambda$, a width of $d=5\lambda$, and dimensionless amplitude $a_0=1$. Note that the deviations from the specified input laser parameters are made in order to account for self-focusing that is usually underestimated by the 2D code. This way, the simulated results fit closer to our observations.

OBSERVATIONS AND DISCUSSIONS

RPA hole boring

Fig. 3 shows typical examples of proton beams recorded on the magnetic spectrometer for $n_e=5-7n_c$, where n_e – plasma density on the axis (under the assumption of full ionization). The most striking observation is the narrow spectral width of the ion feature in these shots especially at highest recorded energy (Fig. 3b) and its scaling proportional to I/n_e , where I is the laser intensity, as is expected for the shock acceleration. In Fig. 3b, the ion beam image is a circle comparable in size to the projected entrance pinhole, indicating that this feature is dominated by the instrument function of the spectrometer. Deconvolution shows the rms energy spread of the beam is as narrow as $\sigma=4\%$.

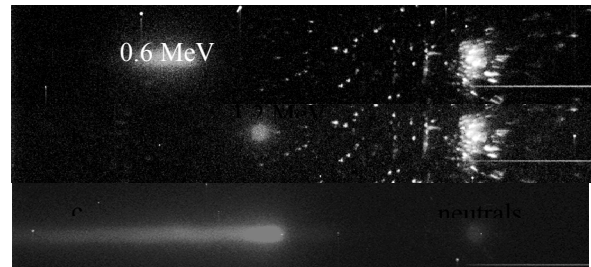


Figure 3: Sample raw spectra seen on spectrometer; a) and b) obtained with a gas jet, c) comparative TNSA spectrum obtained previously from a thin Al foil.

Fig. 4 shows the proton spectrum simulated for our experimental conditions.

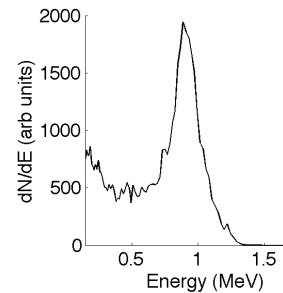


Figure 4: Simulated RPA proton spectrum.

To determine the dynamics of the interaction, simultaneous transverse optical probing was performed. Fig. 5a shows an interferogram taken at $t \approx 50$ ps after arrival of the CO₂ pulse under the conditions when the monoenergetic proton spectrum shown in Fig. 3b has been obtained. A plasma cavity created by the laser inside the gas jet and clearly visible on a simultaneously taken shadowgram (Fig. 5b-top) has a sharp envelope formed

by the critical surface that limits the laser pulse propagation. The resultant radiation pressure causes the critical surface to be driven inwards. Electron plasma density distribution (Fig. 5a-bottom) evaluated from the interferometry pattern shows the plasma within this cavity is at much lower density ($< 10^{18} \text{ cm}^{-3}$). Gas upstream (to

the right) from the moving cavity boundary is just partially ionized. This plasma formation corresponds to hole-boring by the shock driven by the laser radiation pressure at the velocity $v \approx (2I/\rho c)^{1/2}$ [6] that is responsible for monoenergetic peak at the photon energy $\sim I/n_e$. [7]

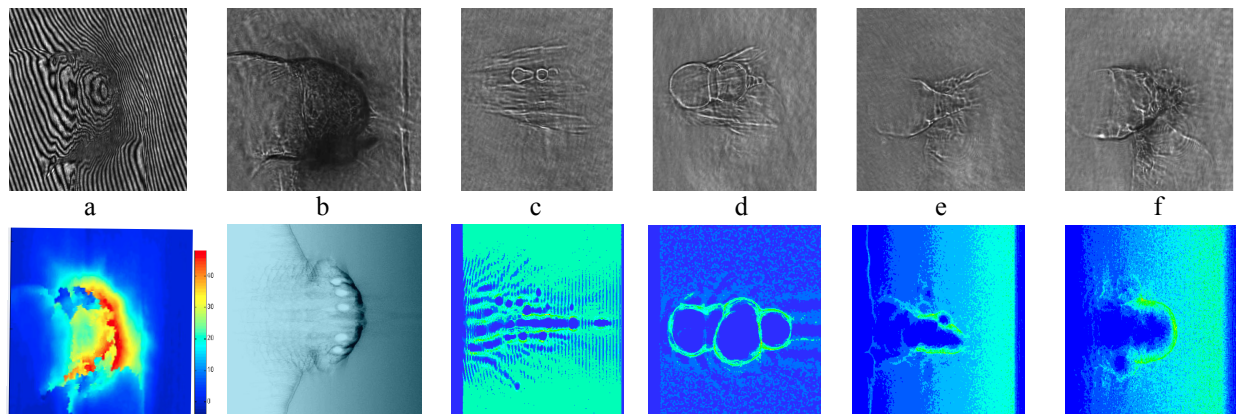


Figure 5: Plasma formations observed in experiment (upper row) and simulated (bottom row) at $t=50$ ps (except(c)); a) interferogram and reconstructed plasma density at $n_e=7n_c$; b) shadowgram and a simulated plasma profile for case (a); c) filamentation and solitons for $n_e < n_c$, $t=7$ ps; d) postsolitons for $n_e < n_c$; e) $n_e=2n_c$; f) $n_e=2.5 n_c$

Post-solitons

At the maximum jet plasma density (assuming full ionization) $< 3 n_c$, the proton energy drops below 0.5 MeV and ceases to display the monoenergetic feature. Simultaneously we see changes in the plasma formations from a smooth hollow channel to the bubble-like structures and filamentation. (Fig. 5c-f). We believe that small plasma bubbles of the order of several laser wavelengths (Fig. 5c) observed in underdense plasma during and immediately after the laser pulse are so-called slow solitons - structures consisting of electron depressions and intense e.m. field concentrations. [8,9] The formation of a soliton is described by trapping of the e.m. energy due to the pulse frequency downshift caused by the pulse depletion. Electrostatic field inside the solitons arises from the charge separation as electrons are pushed outward by the ponderomotive force of the oscillating field. On the longer time scale, the ions are also pushed out, and solitons evolve into quasineutral, slowly expanding post-solitons.[10] The structure observed in Fig. 5d is consistent with post-solitons formed by expansion and merging of several solitons. The last two examples (Fig. 5e-f) illustrate transition between post-soliton to hole-boring regimes. Bubbles open to vacuum while the critical surface at the front serves as the proton emitter.

CONCLUSIONS

The interaction of an intense infrared laser with a gaseous hydrogen target provided the first direct evidence of the high contrast quasi-monoenergetic beams that

have been theorized for RPA. [2,3,11] Optical probing of the laser/plasma interaction revealed hole-boring by the radiation-pressure driven critical surface as well as provided the first detailed post-soliton imaging.

ACKNOWLEDGEMENTS

Authors thank David Neely and Paul McKenna for donating equipment and valuable advices in preparation to this experiment.

REFERENCES

- [1] S. Wilks, et al, Phys. Plasmas 8 (2001) 542.
- [2] T. Esirkerov, et al, Phys. Rev. Lett. 92 (2004) 175003.
- [3] A.P.L. Robinson, et al, New J. Phys. 10 (2008) 0130231.
- [4] J. Fuchs, et al, nat. Phys. 2 (2006) 48.
- [5] L. Willingale, et al, IEEE Trans. Plasma Sci. 36 (2008) 1825.
- [6] S. Wilks, et al, Phys. Rev. Lett. 69 (1992) 1383.
- [7] L. Silva, et al, Phys. Rev. Lett. 92 (2004) 015002.
- [8] T. Esirkepov, et al, Phys. Rev. Lett. 89 (2002) 275002
- [9] M. Borghesi, et al, Phys. Rev. Lett. 88 (2002) 135002
- [10] N.M. Naumova, et. al., Phys. Rev. Lett. 87 (2001) 185004
- [11] T. Liseikina, et al, Plasma Phys. Control. Fusion 50 (2008) 124033.